The Astrophysical Journal Letters, 778:L16 (5pp), 2013 November 20 doi:10.1088/2041-8205/778/1/L16

PROGENITOR MODELS OF THE ELECTROMAGNETIC TRANSIENT ASSOCIATED WITH THE SHORT GAMMA RAY BURST 130603B

Kenta Hotokezaka[1], Koutarou Kyutoku[2], Masaomi Tanaka[3], Kenta Kiuchi[4], Yuichiro Sekiguchi[4], Masaru Shibata[4], and Shinya Wanajo[3]
[1] Department of Physics, Kyoto University, Kyoto 606-8502, Japan
[2] Department of Physics, University of Wisconsin-Milwaukee, P.O. Box 413, Milwaukee, WI 53201, USA
[3] National Astronomical Observatory of Japan, Mitaka, Tokyo, Japan
[4] Yukawa Institute for Theoretical Physics, Kyoto University, Kyoto 606-8502, Japan
Received 2013 October 3; accepted 2013 October 22; published 2013 November 6

ABSTRACT

An electromagnetic transient powered by the radioactive decay of *r*-process elements, a so-called kilonova/macronova, is one of the possible observable consequences of compact binary mergers including at least one neutron star. Recent observations strongly suggest the discovery of the first electromagnetic transient, which is associated with the short gamma ray burst 130603B. We explore a possible progenitor of this event by combining numerical-relativity simulations and radiative transfer simulations of the dynamical ejecta of binary neutron star and black hole–neutron star mergers. We show that the ejecta models within a realistic parameter range consistently reproduce the observed near-infrared excess. We also show that the soft equation-of-state models for binary neutron star mergers and the stiff equation-of-state models for black hole–neutron star mergers are suitable for reproducing the observed luminosity.

Key words: equation of state – gamma-ray burst: general – gamma-ray burst: individual (130603B) – stars: black holes – stars: neutron

Online-only material: color figures

1. INTRODUCTION

Mergers of compact binaries such as binary neutron stars (NS–NSs) and black hole–neutron star binaries (BH–NSs)[5] are candidates for the progenitor of short-hard gamma-ray bursts (GRBs; Paczynski 1986; Goodman 1986; Eichler et al. 1989). As an observable consequence of compact binary mergers, an electromagnetic transient powered by radioactive decay of the heavy elements produced in their ejecta (a so-called kilonova/macronova) was proposed by Li & Paczyński (1998). Recently, strong evidence of an electromagnetic transient associated with the *Swift* short GRB 130603B was observed by the *Hubble Space Telescope* (Tanvir et al. 2013; Berger et al. 2013; de Ugarte Postigo et al. 2013). The observed near-infrared excess is largely consistent with the radioactively powered emission models of NS–NS merger ejecta (Kasen et al. 2013; Barnes & Kasen 2013; Tanaka & Hotokezaka 2013; Grossman et al. 2013).[6] This could be direct evidence for the compact binary merger scenario of short GRBs.

The characteristics of the radioactively powered transient are determined primarily by *r*-process elements which are expected to be produced in the ejecta of compact binary mergers because of their neutron-richness (Lattimer & Schramm 1974; Symbalisty & Schramm 1982; Meyer 1989; Freiburghaus et al. 1999; Goriely et al. 2011; Korobkin et al. 2012; Rosswog et al. 2013b; Bauswein et al. 2013). Decay of the *r*-process elements heats the ejecta and gives rise to an electromagnetic transient emission (Metzger et al. 2010; Roberts et al. 2011; Goriely et al. 2011; Grossman et al. 2013). The *r*-process elements also play an important role as the dominant opacity source of the ejecta. The bound–bound transitions of partially ionized *r*-process elements significantly enhance the opacity of the ejecta in ultraviolet to near-infrared wavelengths (Kasen et al. 2013; Tanaka & Hotokezaka 2013).

The brightness and time scale of an electromagnetic transient depend on the global properties of the ejecta such as the mass, expansion velocity, and morphology. Using the observed data for the near-infrared excess, Berger et al. (2013) estimated the ejecta mass and expansion velocity under the assumption of spherically expanding ejecta. These properties of the ejecta depend on the type of progenitor (NS–NS or BH–NS), parameters of the progenitor models such as the mass and spin of the two objects, and the equation-of-state (EOS) of neutron-star matter. Recent numerical simulations of compact binary mergers have explored ejecta properties (Rosswog et al. 1999; Oechslin et al. 2007; Hotokezaka et al. 2013; Bauswein et al. 2013; Rosswog 2013; Foucart et al. 2013; Lovelace et al. 2013; Kyutoku et al. 2013; Deaton et al. 2013). Based on these numerical studies, we can estimate the dependences of the ejecta properties on the parameters of the progenitor models and on EOSs. Therefore, combining the observed data of the near-infrared excess and the results of numerical simulations, it is possible to constrain the progenitor models of the short GRB 130603B.

In this Letter, we explore possible progenitor models for the electromagnetic transient associated with the short GRB 130603B using our numerical-relativity simulations and radiative transfer simulations of the dynamical ejecta of compact binary mergers. We focus in particular on its dependence on the EOS of neutron-star matter.

2. MASS EJECTION OF COMPACT BINARY MERGERS

The density and velocity structures of the ejecta of compact binary mergers are determined by numerical-relativity

[5] A compact binary implies an NS–NS or BH–NS binary throughout this Letter.
[6] See Jin et al. (2013) for an alternative interpretation, but the non-detection of late-time radio emission of GRB 130603B provides a strong constraint on it (Fong et al. 2013).

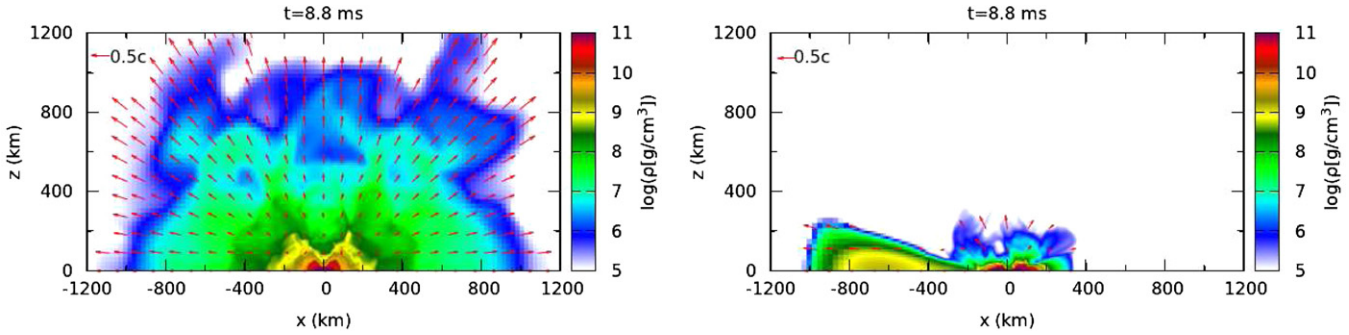

Figure 1. Rest-mass density profiles on the meridional plane for the NS–NS (SLy, $M_{\rm tot} = 2.7 M_\odot$, $Q = 1.0$) (left) and BH–NS (H4, $Q = 3$, $\chi = 0.75$) (right) models at 8.8 ms after the onset of the merger. The red arrows show the velocity profiles of the ejecta.

(A color version of this figure is available in the online journal.)

simulation using SACRA code (Yamamoto et al. 2008). We follow the dynamical ejecta with the numerical-relativity simulation until the head of the ejecta reaches $\simeq$1000 km (see Hotokezaka et al. 2013 and Kyutoku et al. 2013 for details). After that, the density and velocity structures of the ejecta are modeled assuming homologous expansion (Rosswog et al. 2013a). For the simulations, we employ a piecewise polytropic EOS with which the cold EOSs of neutron-star matter are well fitted (Read et al. 2009). For systematic studies of the dependence of mass ejection on the cold EOSs of neutron-star matter, we consider five cold EOSs: APR4 (Akmal et al. 1998) and SLy (Douchin & Haensel 2001) as soft EOSs, ALF2 (Alford et al. 2005) as a moderate EOS, and H4 (Glendenning & Moszkowski 1991; Lackey et al. 2006) and MS1 (Müller & Serot 1996) as stiff EOSs.[7] To take into account the effects of shock heating, we add the thermal pressure as a Γ-law ideal gas EOS. The ejecta masses obtained with this approximation of thermal effects agree with those obtained with tabulated finite-temperature EOSs within errors of several tens of percent for NS–NS mergers (Bauswein et al. 2013).

For NS–NS mergers, we choose the total gravitational mass of the binary $M_{\rm tot} = 2.6\,M_\odot$–$2.8\,M_\odot$ and the mass ratio[8] $Q = 1.0$–1.25. For BH–NS mergers, the gravitational mass of the neutron star $M_{\rm NS}$ is fixed to be $1.35\,M_\odot$ and the mass ratio is chosen to be $Q = 3$–7. The nondimensional spin parameter of the black hole χ is chosen as $\chi = 0.75$. We also perform the simulations for $Q = 7$ and $\chi = 0.5$. These parameters, ejecta masses $M_{\rm ej}$, and averaged ejecta velocities $\langle v_{\rm ej}\rangle/c$ of the progenitor models are summarized in Table 1.

The morphologies of the ejecta for NS–NS and BH–NS mergers are compared in Figure 1. This figure plots the profiles of the density and velocity fields at 8.8 ms after the onset of the merger. Note that the ejecta velocities are in the small range between $\sim 0.1c$ and $\sim 0.3c$ irrespective of the progenitor model. However, the ejecta mass and morphology depend sensitively on the progenitor models. In Table 1, we summarize these properties of the NS–NS and BH–NS ejecta.

NS–NS ejecta. As shown in Figure 1, the NS–NS ejecta have a spheroidal shape, rather than a torus or a disk, irrespective of Q and EOS as long as a hypermassive neutron star is formed after the merger. The reason is as follows. The origin of the

Table 1
Parameters of the Progenitor Models and Their Ejecta Properties

EOS	Type	$R_{1.35}$	$M_{\rm tot}/M_\odot$	Q	χ	$M_{\rm ej}/10^{-2}\,M_\odot$	$\langle v_{\rm ej}\rangle/c$
APR4	NS–NS	11.1	2.6–2.9	1.0–1.25	···	0.01–1.4	0.22–0.27
SLy	NS–NS	11.4	2.6–2.8	1.0–1.25	···	0.8–2.0	0.20–0.26
ALF2	NS–NS	12.4	2.6–2.8	1.0–1.25	···	0.15–0.55	0.22–0.24
H4	NS–NS	13.6	2.6–2.8	1.0–1.25	···	0.03–0.40	0.18–0.26
MS1	NS–NS	14.4	2.6–2.8	1.0–1.25	···	0.06–0.35	0.18–0.20
APR4	BH–NS	11.1	5.4–10.8	3.0–7.0	0.75	0.05–1.0	0.23–0.27
ALF2	BH–NS	12.4	5.4–10.8	3.0–7.0	0.75	2.0–4.0	0.25–0.29
H4	BH–NS	13.6	5.4–10.8	3.0–7.0	0.75	4.0–5.0	0.24–0.29
MS1	BH–NS	14.4	5.4–10.8	3.0–7.0	0.75	6.5–8.0	0.25–0.30
APR4	BH–NS	11.1	10.8	7.0	0.5	$\lesssim 10^{-4}$	···
ALF2	BH–NS	12.4	10.8	7.0	0.5	0.02	0.27
H4	BH–NS	13.6	10.8	7.0	0.5	0.3	0.29
MS1	BH–NS	14.4	10.8	7.0	0.5	1.7	0.30

ejecta for NS–NS mergers can be divided into two parts: the contact interface of two neutron stars at the collision and the tidal tails formed during an early stage of the merger. At the contact interface, the kinetic energy of the approaching velocities of the two stars is converted into thermal energy through shock heating. The heated matter at the contact interface expands into the low-density region. As a result, the shocked matter can escape even toward the rotational axis and the ejecta shape becomes spheroidal. By contrast, the tidal tail component is asymmetric and the ejecta is distributed near the equatorial plane.

Numerical simulations of NS–NS mergers show that the total amount of ejecta is in the range 10^{-4}–$10^{-2}\,M_\odot$ depending on $M_{\rm tot}$, Q, and the EOS (see Figure 2). The more compact neutron star models with soft EOSs produce a larger amount of ejecta, because the impact velocities and subsequent shock heating effects at merger are larger. More specifically, the amount of ejecta is

$$10^{-4} \lesssim M_{\rm ej}/M_\odot \lesssim 2\times 10^{-2} \quad \text{(soft EOSs)},$$
$$10^{-4} \lesssim M_{\rm ej}/M_\odot \lesssim 5\times 10^{-3} \quad \text{(stiff EOSs)}. \qquad (1)$$

Bauswein et al. (2013) show a similar dependence of the ejecta masses on the EOSs and $M_{\rm ej} \lesssim 0.01\,M_\odot$ for stiff EOS models. According to these results, it is worth noting that the ejecta masses of the stiff EOS models are likely to be at most $0.01\,M_\odot$.

The dependence of the ejecta mass on the total mass of the binary is rather complicated as shown in Figure 2. The ejecta mass increases basically with increasing $M_{\rm tot}$ as long

[7] In this Letter, "soft" and "stiff" EOSs mean those which reproduce the radii $R_{1.35} \leqslant 12$ km and $R_{1.35} \geqslant 13.5$ km, respectively. Here $R_{1.35}$ is the radius of a cold, spherical neutron star with the gravitational mass $1.35\,M_\odot$. For all the EOSs, the maximum masses of spherical neutron stars are larger than $\simeq 2\,M_\odot$.

[8] The mass ratio is defined by $Q = m_1/m_2$ with $m_1 \geqslant m_2$, where m_1 and m_2 are the component masses of a binary.

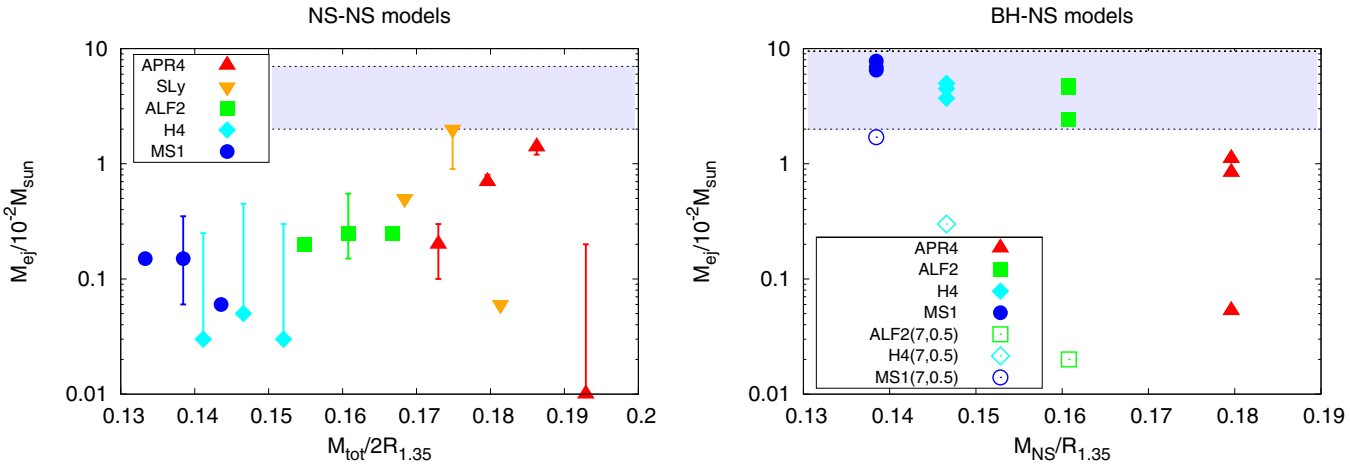

Figure 2. Ejecta masses as a function of the compactness of the neutron star, which is defined by $GM_{\rm tot}/2R_{1.35}c^2$ and $GM_{\rm NS}/R_{1.35}c^2$ for NS–NS and BH–NS models, respectively. Left panel: NS–NS models. Each point shows the ejecta mass for the equal mass cases. Error bars denote the dispersion of the ejecta masses due to the various Q. Right panel: BH–NS models. The filled and open symbols correspond to the models with $(Q, \chi) = (3\text{–}7, 0.75)$ and $(7, 0.5)$, respectively. The blue shaded region in each panel shows the ejecta masses allowed in order to reproduce the observed near-infrared excess of GRB 130603B, $0.02 \lesssim M_{\rm ej}/M_\odot \lesssim 0.07$ and $0.02 \lesssim M_{\rm ej}/M_\odot \lesssim 0.1$ for the NS–NS and BH–NS models, respectively. The lower and upper bounds are imposed by hypothetical high- and low-heating models, respectively.

(A color version of this figure is available in the online journal.)

as a hypermassive neutron star with a lifetime of $\gtrsim$10 ms is formed after the merger. More massive NS–NS mergers result in hypermassive neutron stars with a lifetime of $\lesssim$10 ms or in black holes. For such a case, the ejecta mass decreases with increasing $M_{\rm tot}$ because of the shorter duration of mass ejection.

BH–NS ejecta. Tidal disruption of a neutron star results in anisotropic mass ejection for a BH–NS merger (Kyutoku et al. 2013). As a result, the ejecta is concentrated near the binary orbital plane as shown in Figure 1, and it is shaped like a disk or crescent.

The amount of ejecta for the BH–NS models is smaller for more compact neutron star models with fixed values of χ and Q as shown in Figure 2. This is because tidal disruption occurs in a less significant manner. This dependence of the BH–NS ejecta on the compactness of neutron stars is opposite to the case of the NS–NS ejecta.

More specifically, the amount of ejecta is

$$5 \times 10^{-4} \lesssim M_{\rm ej}/M_\odot \lesssim 10^{-2} \quad \text{(soft EOSs)},$$
$$4 \times 10^{-2} \lesssim M_{\rm ej}/M_\odot \lesssim 7 \times 10^{-2} \quad \text{(stiff EOSs)}, \qquad (2)$$

for $\chi = 0.75$ and $3 \leqslant Q \leqslant 7$. For $\chi = 0.5$, the ejecta mass is smaller than that for $\chi = 0.75$. Only the stiff EOS models can produce large amounts of ejecta more than 0.01 $M_\odot$ for $\chi = 0.5$ and $Q = 7$.

For both NS–NS and BH–NS merger models, winds driven by neutrino/viscous/nuclear-recombination heating or the magnetic field from the central object might provide ejecta in addition to the dynamical ejecta (Dessart et al. 2009; Wanajo & Janka 2012; Kiuchi et al. 2012; Fernández & Metzger 2013). However, it is not easy to estimate the amount of wind ejecta, because it depends strongly on the condition of the remnant formed after the merger. In this Letter, we focus only on the dynamical ejecta.

3. RADIATIVE TRANSFER SIMULATIONS FOR THE EJECTA

For the NS–NS and BH–NS merger models described in Section 2, we perform radiative transfer simulations to obtain the light curves of the radioactively powered emission from the ejecta using the three-dimensional, time-dependent, multi-frequency Monte Carlo radiative transfer code (Tanaka & Hotokezaka 2013). For a given density structure of the ejecta and elemental abundances, this code computes the emission in the ultraviolet, optical, and near-infrared wavelength ranges by taking into account the detailed r-process opacities. In this Letter, we include r-process elements with $Z \geqslant 40$ assuming the solar abundance ratios by Simmerer et al. (2004). More details of the radiation transfer simulations are described in Tanaka & Hotokezaka (2013); Tanaka et al. (2013).

The heating rate from the radioactive decay of r-process elements is one of the important ingredients of radiative transfer simulations. As a fiducial-heating model, we employ the heating rate computed with the abundance distribution that reproduces the solar r-process pattern (see Tanaka et al. 2013 for more detail). Heating is due to β-decays only, which increase atomic numbers from the neutron-rich region toward the β-stability line without changing the mass number A. This heating rate is in reasonable agreement with those from previous nucleosynthesis calculations (Metzger et al. 2010; Goriely et al. 2011; Grossman et al. 2013) except for the first several seconds.

We note that quantitative uncertainties could exist in the heating rate as well as in the opacities. As an example, the heating rate would be about a factor 2 higher if the r-process abundances of $A \sim 130$ (or those produced with the electron fraction of $Y_{\rm e} \sim 0.2$) were dominant in the ejecta (Metzger et al. 2010; Grossman et al. 2013). To take into account such uncertainties, we also consider the cases in which the light curves of mergers are twice and half as luminous (high- and low-heating models; only explicitly shown for the NS–NS models in Figure 3) as those computed with the fiducial-heating model.

4. LIGHT CURVES AND POSSIBLE PROGENITOR MODELS

The computed light curves and observed data in r and H-band are compared in Figure 3. The left panel of Figure 3 shows the light curves of the NS–NS merger models SLy

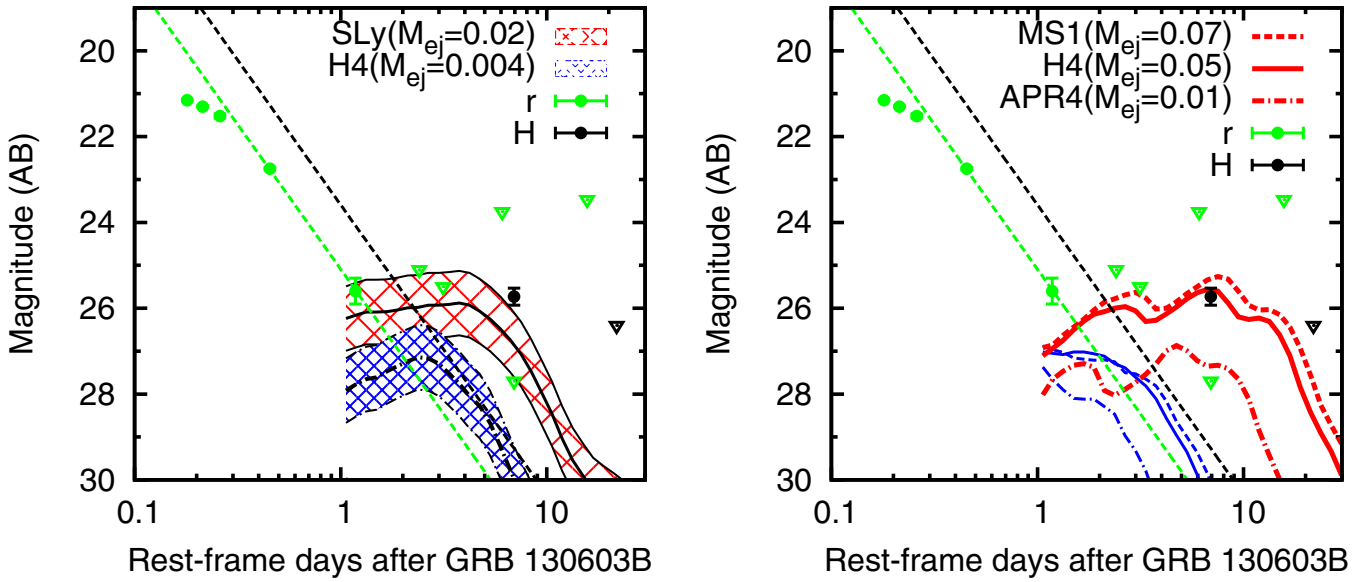

Figure 3. Predicted light curves for NS–NS and BH–NS models. Left panel: NS–NS models. The dashed, solid, and dot-dashed curves show the H-band light curves for the models: SLy ($Q = 1.0$, $M_{\rm ej} = 0.02\,M_\odot$), H4 ($Q = 1.25$, $M_{\rm ej} = 4 \times 10^{-3}\,M_\odot$), respectively. The total mass of the progenitor is fixed to be $2.7\,M_\odot$. The upper, middle, and lower curves for each model correspond to the high-, fiducial- and low-heating models. Right panel: BH–NS models. The dashed, solid, and dot-dashed curves show the models MS1 ($M_{\rm ej} = 0.07\,M_\odot$), H4 ($M_{\rm ej} = 0.05\,M_\odot$), and APR4 ($M_{\rm ej} = 0.01\,M_\odot$), respectively. Here only the fiducial-heating models are shown. The thin and thick lines denote the r and H-band light curves. Here we set $(Q, \chi) = (3, 0.75)$. The observed data (filled circles), upper limits (triangles), and the light curves (dashed lines) of the afterglow model of GRB 130603B in r and H-band are plotted (Tanvir et al. 2013; de Ugarte Postigo et al. 2013). The observed point in the r-band at 1 days after the GRB is consistent with the afterglow model. The key observations for an electromagnetic transient are the observed H-band data at 7 days after the GRB, which exceed the H-band light curve of the afterglow model, and the upper limit in H-band at 22 days after the GRB. These data suggest the existence of an electromagnetic transient associated with GRB 130603B.

(A color version of this figure is available in the online journal.)

($Q = 1.0$, $M_{\rm ej} = 0.02\,M_\odot$) and H4 ($Q = 1.25$, $M_{\rm ej} = 4 \times 10^{-3}\,M_\odot$) for reference. Here the total mass of the progenitor is chosen to be $M_{\rm tot} = 2.7\,M_\odot$. We plot three light curves derived with the fiducial- (the middle curves), high- (the upper curves), and low-heating models (the lower curves). We expect that the realistic light curves may lie within the shaded regions. For the NS–NS models, the computed r-band light curves are fainter than 30 mag. The right panel of Figure 3 shows the light curves of the BH–NS merger models, MS1 ($M_{\rm ej} = 0.07\,M_\odot$), H4 ($M_{\rm ej} = 0.05\,M_\odot$), and APR4 ($M_{\rm ej} = 0.01\,M_\odot$) with $(Q, \chi) = (3, 0.75)$. For these cases, we employ the fiducial-heating model. Note that the r-band light curves of the BH–NS models reach $\sim$27 mag, which implies that the light curves of the BH–NS models are bluer than those of the NS–NS models. This is because the energy from radioactive decay is deposited into a small volume for the BH–NS models (see Tanaka et al. 2013 in details). As shown in Figure 6 of Kasen et al. (2013, see also Figure 15 of Tanaka & Hotokezaka 2013), the opacity of r-process elements depends strongly on the temperature, and thus the time after the merger. The small bumps in the H-band light curves of BH–NS models are caused by this time-dependent opacity.

Uncertainties are expected to be associated with the difference in the morphology between the models of the same progenitor type but different masses and spins. Moreover, the light curves may depend on the viewing angle. However, these uncertainties are not large enough to significantly affect our results (see Tanaka & Hotokezaka 2013; Tanaka et al. 2013 for details).

We now translate these results into the progenitor models as Q, χ, and EOS.

NS–NS models. The NS–NS models for GRB 130603B should have ejecta of mass $\gtrsim 0.02\,M_\odot$. This is consistent with that derived by Berger et al. (2013). This value strongly constrains the NS–NS models because the amount of ejecta is at most $\sim 0.02\,M_\odot$ for an NS–NS merger within the plausible mass range of the observed NS–NS systems (Özel et al. 2012). Specifically, as shown in Figure 2, such a large amount of ejecta can be obtained only for the soft EOS models in which a hypermassive neutron star with a lifetime of $\gtrsim$10 ms is formed after the merger. For the stiff EOS models, the amount of ejecta is at most $4 \times 10^{-3}\,M_\odot$. Thus we conclude that the ejecta of the NS–NS models with soft EOSs ($R_{1.35} \lesssim 12$ km) are favored as the progenitor of GRB 130603B.

BH–NS models. The observed data in the H-band is consistent with the BH–NS models which produce the ejecta of $\sim 0.05\,M_\odot$ in our fiducial-heating model. Such a large amount of ejecta can only be obtained with the stiff EOSs ($R_{1.35} \gtrsim 13.5$ km) for the case of $\chi = 0.75$ and $3 \leqslant Q \leqslant 7$ as shown in Figure 2. For the soft EOS models, the total amount of ejecta reaches only $0.01\,M_\odot$ as long as $\chi \leqslant 0.75$, which hardly reproduces the observed near-infrared excess. Thus the models with stiff EOSs are favored for the BH–NS merger models as the progenitor model of GRB 130603B as long as the parameters satisfy $0.5 \leqslant \chi \leqslant 0.75$ and $3 \leqslant Q \leqslant 7$. It is worth noting that any BH–NS models with $\chi \leqslant 0.5$ and $Q \geqslant 7$ are unlikely to reproduce the observed near-infrared excess.

5. DISCUSSION AND CONCLUSION

We explored possible progenitor models of the electromagnetic transient associated with the *Swift* short GRB 130603B. This electromagnetic transient may have been powered by the radioactive decay of r-process elements, a so called kilonova/macronova. We analyzed the dynamical ejecta of NS–NS and BH–NS mergers for the progenitor models of this event. To

compute the expected light curves, we carried out radiative transfer simulations using density and velocity structures obtained from numerical-relativity simulations with several total masses, mass ratios, and EOSs. Depending on these quantities, the total amount of ejecta mass varies by orders of magnitude $10^{-4}\,M_{\odot}$ to $10^{-2}\,M_{\odot}$ for the NS–NS models and $10^{-5}\,M_{\odot}$ to $10^{-1}\,M_{\odot}$ for the BH–NS models.

For both NS–NS and BH–NS models, we found that there are progenitor models that can reproduce the observed near-infrared excess within the realistic parameter ranges. Specifically, the observed data suggest that the required ejecta mass is at least $\sim 0.02\,M_{\odot}$ for NS–NS mergers. For BH–NS mergers, the required ejecta mass would be $\sim$0.02–0.1 $M_{\odot}$ taking into account the uncertainty in the heating rate and opacities. These values are consistent with the results of a spherically expanding ejecta model (Berger et al. 2013). Such a large amount of material is ejected when a hypermassive neutron star with a lifetime of $\gtrsim$10 ms is formed after the merger for the NS–NS models and when the neutron star is tidally disrupted for the BH–NS models. For these cases, the merger results in a spinning black hole surrounded by a massive torus $\sim 0.1\,M_{\odot}$. Such a remnant could have been the central engine of GRB 130603B.

We constrained the progenitor models of GRB 130603B, which should produce the required amount of ejecta. We found that the soft EOS models are more favorable for NS–NS models. For BH–NS models with a mass ratio of $3 \leqslant Q \leqslant 7$ and a nondimensional spin parameter for the black hole of $0.5 \leqslant \chi \leqslant 0.75$, the stiff EOS models are favorable. For $\chi \leqslant 0.5$, any BH–NS models with $Q \geqslant 7$ are unlikely to produce the required amount of ejecta. These results may be valid as long as the mass ejection due to winds is subdominant. In future, observations of gravitational waves from compact binary mergers within $\sim$200 Mpc will provide the masses of the binaries and their types. Combining the observations of the gravitational-wave and electromagnetic signals, it will be possible to constrain more stringently the progenitor models, in particular the EOSs, of such events.

We thank T. Nakamura for fruitful discussions. This work was supported by Grant-in-Aid for Scientific Research (21340051, 23224004, 23750160, 24244028, 24740117, 24740163, 25103510, 25105508, 25103512) by Grant-in-Aid for Scientific Research on Innovative Area (20105004, 25103515), HPCI Strategic Program of Japanese MEXT, and "Joint Usage/Research Center for Interdisciplinary Large-scale Information Infrastructures" in Japan. The work of K. Hotokezaka and K. Kyutoku is supported by a JSPS fellowship and JSPS Postdoctoral Fellowship for Research Abroad. The numerical simulations presented in this Letter were in part carried out with Cray XC30 at the Center for Computational Astrophysics, National Astronomical Observatory of Japan. This work was carried out, in part, in the long-term workshop on *Gravitational Waves and Numerical Relativity* at the Yukawa Institute for Theoretical Physics.

REFERENCES

Akmal, A., Pandharipande, V. R., & Ravenhall, D. G. 1998, PhRvC, 58, 1804
Alford, M., Braby, M., Paris, M., & Reddy, S. 2005, ApJ, 629, 969
Barnes, J., & Kasen, D. 2013, ApJ, 775, 18
Bauswein, A., Goriely, S., & Janka, H.-T. 2013, ApJ, 773, 78
Berger, E., Fong, W., & Chornock, R. 2013, ApJL, 774, L23
de Ugarte Postigo, A., Thoene, C. C., Rowlinson, A., et al. 2013, arXiv:1308.2984
Deaton, M. B., Duez, M. D., Foucart, F., et al. 2013, ApJ, 776, 47
Dessart, L., Ott, C. D., Burrows, A., Rosswog, S., & Livne, E. 2009, ApJ, 690, 1681
Douchin, F., & Haensel, P. 2001, A&A, 380, 151
Eichler, D., Livio, M., Piran, T., & Schramm, D. N. 1989, Natur, 340, 126
Fernández, R., & Metzger, B. D. 2013, MNRAS, 435, 502
Fong, W.-f., Berger, E., Metzger, B. D., et al. 2013, arXiv:1309.7479
Foucart, F., Deaton, M. B., Duez, M. D., et al. 2013, PhRvD, 87, 084006
Freiburghaus, C., Rosswog, S., & Thielemann, F.-K. 1999, ApJL, 525, L121
Glendenning, N. K., & Moszkowski, S. A. 1991, PhRvL, 67, 2414
Goodman, J. 1986, ApJL, 308, L47
Goriely, S., Bauswein, A., & Janka, H.-T. 2011, ApJL, 738, L32
Grossman, D., Korobkin, O., Rosswog, S., & Piran, T. 2013, arXiv:1307.2943
Hotokezaka, K., Kiuchi, K., Kyutoku, K., et al. 2013, PhRvD, 87, 024001
Jin, Z.-P., Xu, D., Fan, Y.-Z., Wu, X.-F., & Wei, D.-M. 2013, ApJL, 775, L19
Kasen, D., Badnell, N. R., & Barnes, J. 2013, ApJ, 774, 25
Kiuchi, K., Kyutoku, K., & Shibata, M. 2012, PhRvD, 86, 064008
Korobkin, O., Rosswog, S., Arcones, A., & Winteler, C. 2012, MNRAS, 426, 1940
Kyutoku, K., Ioka, K., & Shibata, M. 2013, PhRvD, 88, 041503
Lackey, B. D., Nayyar, M., & Owen, B. J. 2006, PhRvD, 73, 024021
Lattimer, J. M., & Schramm, D. N. 1974, ApJL, 192, L145
Li, L.-X., & Paczyński, B. 1998, ApJL, 507, L59
Lovelace, G., Duez, M. D., Foucart, F., et al. 2013, CQGra, 30, 135004
Metzger, B. D., Martínez-Pinedo, G., Darbha, S., et al. 2010, MNRAS, 406, 2650
Meyer, B. S. 1989, ApJ, 343, 254
Müller, H., & Serot, B. D. 1996, NuPhA, 606, 508
Oechslin, R., Janka, H.-T., & Marek, A. 2007, A&A, 467, 395
Özel, F., Psaltis, D., Narayan, R., & Santos Villarreal, A. 2012, ApJ, 757, 55
Paczynski, B. 1986, ApJL, 308, L43
Read, J. S., Lackey, B. D., Owen, B. J., & Friedman, J. L. 2009, PhRvD, 79, 124032
Roberts, L. F., Kasen, D., Lee, W. H., & Ramirez-Ruiz, E. 2011, ApJL, 736, L21
Rosswog, S. 2013, RSPTA, 371, 20272
Rosswog, S., Korobkin, O., Arcones, A., & Thielemann, F.-K. 2013a, arXiv:1307.2939
Rosswog, S., Liebendörfer, M., Thielemann, F.-K., et al. 1999, A&A, 341, 499
Rosswog, S., Piran, T., & Nakar, E. 2013b, MNRAS, 430, 2585
Simmerer, J., Sneden, C., Cowan, J. J., et al. 2004, ApJ, 617, 1091
Symbalisty, E., & Schramm, D. N. 1982, ApL, 22, 143
Tanaka, M., & Hotokezaka, K. 2013, ApJ, 775, 113
Tanaka, M., Hotokezaka, K., Kyutoku, K., et al. 2013, arXiv:1310.2774
Tanvir, N. R., Levan, A. J., Fruchter, A. S., et al. 2013, Natur, 500, 547
Wanajo, S., & Janka, H.-T. 2012, ApJ, 746, 180
Yamamoto, T., Shibata, M., & Taniguchi, K. 2008, PhRvD, 78, 064054